PERGAMON

International Journal of Heat and Mass Transfer 44 (2001) 2863–2875

International Journal of HEAT and MASS TRANSFER

www.elsevier.com/locate/ijhmt

Effect of free stream turbulence on local mass transfer from a circular cylinder

S. Sanitjai, R.J. Goldstein *

Heat Transfer Laboratory, University of Minnesota-Twin Cities, Institute of Technology, Department of Mechanical Engineering, 125 Mechanical Engineering Building, 111 Church Street S.E., Minneapolis, MN 55455-0111, USA

Received 1 March 2000; received in revised form 11 October 2000

Abstract

The effect of free stream turbulence on local mass transfer from a circular cylinder is experimentally investigated for free stream Reynolds number from 3.0×10^4 to 8.3×10^4, turbulence intensity from 0.2% to 23.7% and integral length scale from 0.8 to 6.3 cm. The pattern of mass transfer distribution changes considerably with free stream turbulence. The effect of a splitter plate on local mass transfer is also studied. Information on the flow field near the surface is obtained from flow visualization using an oil/lampblack mixture.

1. Introduction

Heat and mass transfer from a circular cylinder have been extensively studied (cf. [1]). In many applications such as heat exchanger design, detailed information regarding the circumferential and longitudinal variation of heat transfer to a cylinder is required. The major parameters that affect the heat (mass) transfer coefficient are the Reynolds number, the Prandtl (Schmidt) number, surface roughness, turbulence intensity and length scale.

Experiments have shown that heat transfer is often augmented by the free stream turbulence. Giedt [2] measured the local heat transfer coefficients on a circular cylinder placed normal to an air stream. He observed a larger rate of heat transfer in the laminar boundary layer on the front part of the cylinder with increased free stream turbulence. Bollen [3] and Zapp [4] reported that increasing free stream turbulence lowers the critical Reynolds number (from $Re_c \approx 2 \times 10^5$, Morkovin [5]) at which transition occurs in the boundary layer flow producing a later (larger θ) flow separation. Seban [6], Kestin and Maeder [7] and Kestin et al. [8] found larger turbulence intensity produces higher heat transfer coefficients (at different locations on a cylinder) through a direct increase in heat transfer to the laminar boundary layer, through an earlier transition to turbulence or through substantial changes in the characteristics of the separated flow. Over a range of Reynolds number near the critical value (Re_c), the effects of turbulence on heat transfer in air and water flow were investigated by Zukauskas et al. [9]. They found that the turbulence effects depend on Prandtl number in water and are smaller than in air.

Recently, Lee et al. [10], using naphthalene mass transfer, reported that at low turbulence intensity the local Sherwood number (Sh) distribution qualitatively shows the trend of the typical subcritical flow with no turbulence, but at higher turbulence level the distribution of Sherwood number changes drastically. Two minima in Sh vs. position (θ) around the cylinder were found, similar to those observed in the supercritical flow regime ($Re > 3.5 \times 10^6$, Morkovin [5]). Scholten and Murray [11] measured the instantaneous and time-averaged heat flux around a circular cylinder. The fluctuation and the auto spectra of the heat flux under high free stream turbulence were examined.

Heat transfer from a circular cylinder can be affected by the integral length scale (L_x). Zijnen [12] found a maximum increase in heat transfer at $L_x/d \approx 1.6$. Yardi and Sukhatme [13] found a greater increase in the heat transfer coefficient at the front stagnation point for smaller values of L_x/d than for larger values of L_x/d at the same value of the turbulence parameter $Tu\,Re^{1/2}$.

* Corresponding author. Tel.: +1-612-625-5552; fax: +1-612-625-3434.

E-mail address: rjg@me.umn.edu (R.J. Goldstein).

0017-9310/01/$ - see front matter
PII: S0017-9310(00)00315-X

Nomenclature

A_g	total (metal or wood) blocked area on the grid turbulence generator, m^2
A_t	cross-sectional area of the test section, m^2
AR	open area ratio (A_g/A_t) of turbulence generators
c_p	specific heat, J/(kg K)
D_{na}	binary diffusion coefficient of naphthalene in air (Eq. (6)), m^2/s
d	diameter of circular cylinder ($d = 50$ mm in present study), m
E_1	one-dimensional energy spectrum (Eq. (11)), m^2/s
f	frequency (Eq. (11)), 1/s
h	heat transfer coefficient (Eq. (17)), W/(m^2 K)
h_m	naphthalene mass transfer coefficient (Eq. (1)), m/s
k	thermal conductivity of air, W/(m K)
L_x	longitudinal integral length scale (Eq. (13)), m
l	cylinder length ($l = 275$ mm in present study), m
$\dot{m}$	mass transfer rate per unit area (Eq. (2)), kg/(m^2 s)
n	power index used in Eq. (17)
Nu	Nusselt number, $Nu = hd/k$
P_{atm}	atmospheric pressure, Pa
$P_{n,w}$	naphthalene saturated vapor pressure at the surface (Eq. (4)) ($P_{n,w}$@28°C ≈ 16.67 Pa)
Pr	Prandtl number, $Pr = \mu c_p/k$
R	autocorrelation coefficient (Eq. (10))
R_{11}	longitudinal correlation of u'-fluctuation (Eq. (14))
R_n	gas constant for naphthalene ($R_n = 64.87$ Nm/kg K)
Re	Reynolds number, $Re = Ud/v$
Re_c	critical Reynolds number, $Re_c \approx 2 \times 10^5$
Sc	Schmidt number, $Sc = v/D_{na} \approx 2.28$
Sh	Sherwood number, $Sh = h_m d/D_{na}$
Sh_{avg}	average Sherwood number
$Sh_{\theta=0}$	Sherwood number at front stagnation line
$Sh_{\theta=180}$	Sherwood number at rear stagnation line
T_{dy}	dynamic temperature, K
$T_{n,w}$	naphthalene surface temperature, K
T_r	recovery temperature, K
T_∞	free stream temperature, K
Tu	turbulence intensity, $Tu = \sqrt{\overline{u'^2}}/U$
U	local average velocity, m/s
U_c	average velocity at $x/d = 0$, $y/d = 0$ and $z/d = 4.57$, m/s
U_{in}	inlet velocity, m/s
u	longitudinal velocity, m/s
u'	fluctuation of longitudinal velocity, m/s
W	width and height of the test section ($W = 457$ mm in present study, cf. Fig. 1), m
x	distance in streamwise direction measured from cylinder axis, m
$\vec{x}$	position vector (Eq. (10))
y	distance in cross-stream direction measured from cylinder axis, (tunnel walls at $y/d = \pm 4.57$), m
z	distance in spanwise direction measured from bottom wall, (tunnel walls at $z/d = 0, 9.14$), m

Greek symbols

$\triangle(Sh/\sqrt{Re})$	difference in Sherwood number between low and high free stream turbulence flow, $\triangle\left(Sh/\sqrt{Re}\right) = \left[\left(\left(Sh/\sqrt{Re}\right) - \left(Sh_{Tu=0.2}/\sqrt{Re_{Tu=0.2}}\right)\right)\Big/ \left(Sh_{Tu=0.2}/\sqrt{Re_{Tu=0.2}}\right)\right]$
$\delta\tau$	duration of exposing naphthalene to flow, s
δt	net naphthalene sublimed depth, m
θ	angle around the cylinder, $\theta = 0°$ at front stagnation line
μ	dynamic viscosity of air, kg/(m s)
v	kinematic viscosity of air, m^2/s
$\rho_{n,w}$	concentration of naphthalene vapor at a wall, kg/m^3
$\rho_{n,\infty}$	concentration of naphthalene vapor in the approaching flow, kg/m^3
ρ_s	density of solid naphthalene, $\rho_s = 1450$ kg/m^3
τ	time, s

The heat transfer coefficient at the rear stagnation point was unaffected by the free stream turbulence. Length scale generally has been found to have a small effect on the average heat transfer coefficient. However, Torii and Yang [14] found that the Nusselt number at the rear stagnation point varies with the relative scale L_x/d. At the same Reynolds number, the laminar-to-turbulent transition in the separated shear layer moves downstream with increasing relative scale L_x/d. Recently, Van Fossen et al. [15] studied the effects of free stream tur-

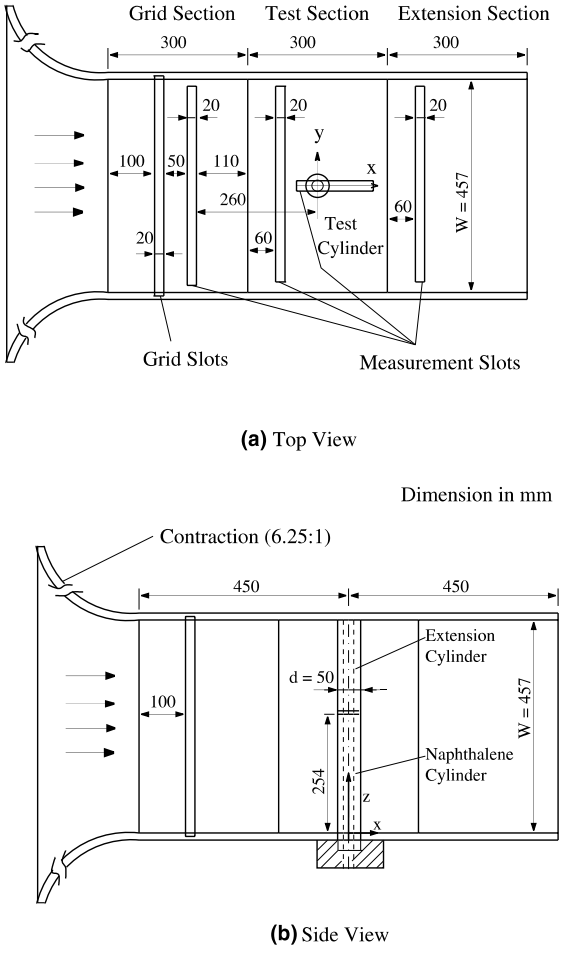

Fig. 1. Test cylinder and test section (dimension in mm).

bulence intensity, length scale, Reynolds number and leading-edge velocity gradient on the front stagnation region heat transfer. They found that heat transfer in the front stagnation region increases with decreasing length scale.

Some empirical correlations for heat transfer near the front stagnation point have been proposed by Smith and Kuethe [16] and Ames [17]. Van Fossen et al. [15] proposed a correlation for the front stagnation heat transfer for isotropic turbulence as a function of $TuRe^{0.8}(L_x/d)^{-0.574}$.

For high free stream turbulence levels, the results from many studies show considerable discrepancies believed to come from several sources, such as differences in the decay rate of turbulence even at the same turbulence intensity and in the integral length scale of turbulence. Few researchers (cf. Van Fossen et al. [15]) have studied the effect of both high free stream turbulence ($Tu > 15\%$) and large longitudinal integral length scale ($L_x/d > 0.5$) on local heat (mass) transfer from a circular cylinder.

The present study provides information on the effect of the turbulence intensity and length scale on local mass transfer. The investigation includes measurements with and without a splitter plate at the rear stagnation line of the cylinder. The naphthalene sublimation technique is used to measure local mass transfer coefficients. Flow visualization provides some understanding of the flow field around the cylinder.

The combined effect of turbulence intensity and longitudinal integral length scale on local mass transfer is investigated over a limited Reynolds number $3.0 \times 10^4 < Re < 8.3 \times 10^4$ for $0.2\% < Tu < 23.7\%$ and $0.8\ \text{cm} < L_x < 6.3\ \text{cm}$. An oil/lampblack technique provides flow visualization results at Reynolds number of 6×10^4.

2. Experimental apparatus and instrumentation

The experiments are conducted in a blowing-type wind tunnel. The inlet to the test section has an area contraction ratio of 6.25. The exit velocity from the contraction, in the absence of a turbulence generator and the test cylinder, is about 40 m/s with turbulence intensity of about 0.2%. With the cylinder present the free stream velocity was 19.4 m/s for Re of 6.0×10^4. The turbulence generator section placed downstream of the contraction nozzle has a cross section of 45.7 cm by 45.7 cm. The test section follows and has the same cross section and a 30 cm length.

The wind tunnel test section and a cylindrical naphthalene test piece are shown in Fig. 1. The cylinder is aluminum with a diameter of 50 mm, and a total length of 275 mm. Except in the region near the ends, a recess 2 mm deep and 250 mm long is machined on the outer surface of the test cylinder. Molten naphthalene is cast in this recess. Thermocouples installed in the naphthalene measure the temperature near the outer surface. Two metal rims at the ends of the cylinder are used as bounding surfaces in the casting process and as reference locations in the surface profile measurement. The test cylinder, with an extension cylinder (white derlin, 50 mm in diameter and 194.9 mm long) on top, is placed vertically in the middle of the test section during its exposure to the air stream. The blockage ratio (d/W) is 0.11.

Four turbulence generators are used. Three are grids shown in Fig. 2. The other is a combustor-like turbulence generator described by Wang [18].

3. Experimental technique

Analyzed Reagent Grade naphthalene ($C_{10}H_8$) powder (0.0008% residue after ignition) manufactured by

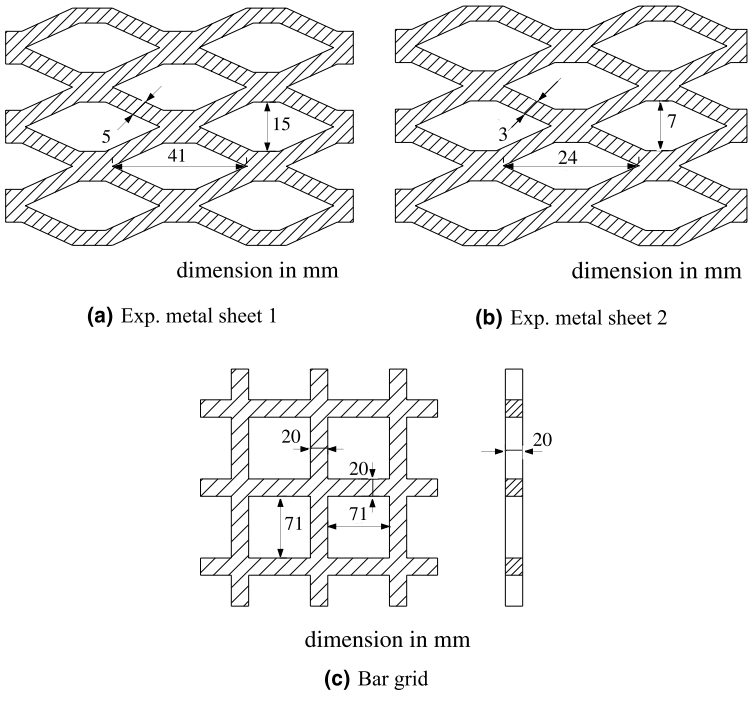

(a) Exp. metal sheet 1

(b) Exp. metal sheet 2

(c) Bar grid

Fig. 2. Turbulence generators.

Baker Chemical Co. is used as the subliming material. Molten naphthalene poured in the recess through the naphthalene-filling hole in the casting system flows out with air through the air vent hole. After the naphthalene solidifies, the mold is separated and the metal rims are cleaned. The technique produces a smooth and clean surface.

The naphthalene surface profile before and after exposure in the wind tunnel is measured using an automated data acquisition system. The sublimation depth is calculated from the differences in the two profiles. A Linear Variable Differential Transformer depth gauge (Schaevitz PCA-200-010 LVDT) moves across the surface using an automated traversing system. The test cylinder is in an enclosure saturated with naphthalene vapor to reduce natural convection sublimation. The rotary table (θ-table) rotates the cylinder to the desired angle. The depth gauge is fixed to the linear-axis table (y-table) which moves along the axis of the cylinder. The rate of measurement is above 3000 points per hour. Reference lines between points on the metal rims are defined. The differences in elevation relative to the reference lines are measured at the same locations before and after the wind tunnel run, which give the naphthalene loss by sublimation.

The Sherwood number, Sh is determined from the naphthalene loss. The boundary condition is analogous to a constant temperature surface in a heat transfer experiment because the saturated vapor pressure of naphthalene at the surface is essentially constant.

The local mass transfer coefficient, h_m, is defined as:

$$h_m = \frac{\dot{m}}{(\rho_{n,w} - \rho_{n,\infty})}. \tag{1}$$

The mass transfer rate per unit area is determined from the net sublimation loss of naphthalene during exposure to the flow:

$$\dot{m} = \frac{\rho_s \, \delta t}{\delta \tau}. \tag{2}$$

The net sublimation is the difference in depth between the first and the second profile measurements, corrected by the loss from natural convection sublimation which is experimentally determined.

Since the incoming air has no naphthalene vapor, $\rho_{n,\infty}$ is zero and Eq. (1) reduces to

$$h_m = \frac{\rho_s \, (\delta t/\delta \tau)}{\rho_{n,w}}. \tag{3}$$

The vapor density of naphthalene at the wall is determined using the ideal gas law

$$\rho_{n,w} = \frac{P_{n,w}}{R_n \, T_{n,w}}, \tag{4}$$

where $P_{n,w} \approx 16.67$ N/m^2, $R_n = 64.87$ Nm/kg K. At the largest Re ($Re \approx 8.3 \times 10^4$, $U_{in} \approx 27$ m/s and $T_{dy} \approx 0.35$°C) the variation in recovery temperature (T_r) around the cylinder has a small impact on the properties

of naphthalene. This primarily affects the results in the rear of the cylinder ($120° < \theta < 180°$). Correction for this at the highest velocity increases the Sh by a maximum of 3%.

Using the local mass transfer coefficient, the cylinder size, the properties of naphthalene, the local Sherwood number is calculated,

$$Sh = \frac{h_m d}{D_{na}}, \tag{5}$$

where D_{na} is calculated using Eq. (6) recommended in [19]

$$D_{na} = 6.81 \times 10^{-6} \left(\frac{T_\infty}{298.15} \right)^{1.93} \frac{1.01325 \times 10^5}{P_{atm}}. \tag{6}$$

Uncertainty in this experiment is analyzed using the method described by Coleman and Steele [20]. It is evaluated based on the 95% confidence level. The uncertainty in mass transfer coefficient is 4.5% and in Sherwood number is 6.8%.

4. Flow field measurement

The turbulent flow velocity includes an average velocity and a fluctuating velocity,

$$u(\vec{x}, \tau) \equiv U(\vec{x}) + u'(\vec{x}, \tau). \tag{7}$$

Turbulence intensity is defined as

$$Tu \equiv \frac{\sqrt{\overline{u'^2}}}{U}, \tag{8}$$

where

$$\sqrt{\overline{u'^2}} \equiv \left(\lim_{\tau \to \infty} \frac{1}{\tau} \int_0^\tau u'^2 \, dt \right)^{1/2}. \tag{9}$$

The autocorrelation determined using a single hot-wire probe is defined as

$$R(\vec{x}, (\tau + \tau_1) - \tau) \equiv \frac{\overline{u'(\vec{x}, \tau) u'(\vec{x}, \tau + \tau_1)}}{\overline{u'^2}}, \tag{10}$$

where the average is taken with respect to time τ.

The correlation function and the energy density spectrum are Fourier cosine transforms. The correlation function can be obtained from the energy density spectrum and vice versa [18],

$$E_1(f) = 4\overline{u'^2} \int_0^\infty R(\tau) \cos(2\pi f \tau) \, d\tau, \tag{11}$$

$$R(\tau) = \frac{1}{\overline{u'^2}} \int_0^\infty E_1(f) \cos(2\pi f \tau) \, df. \tag{12}$$

The turbulence is assumed to be homogeneous and isotropic. Taylor's hypothesis is applied to obtain the length scale. In this experiment all turbulence parameters are calculated under this assumption. By the definition of correlation functions, the longitudinal integral length scale of u'-fluctuation (correlated in x-direction of u'-component) can be computed as follows [18]:

$$L_x \equiv \int_0^\infty R_{11}(x) \, dx = \frac{U E_1(0)}{4\overline{u'^2}}, \tag{13}$$

where R_{11} is longitudinal correlation of u'-fluctuation defined as:

$$R_{11}((x + x_1) - x, y) \equiv \frac{\overline{u'(x) u'(x + x_1)}}{\sqrt{\overline{(u'(x))^2}} \sqrt{\overline{(u'(x + x_1))^2}}}. \tag{14}$$

For isotropic and homogeneous turbulence, the relation between $R(\tau)$ and $R_{11}(x)$ is

$$R(\tau) \cong R_{11}(x)_{x = U\tau}. \tag{15}$$

The flow field is measured using a single-sensor constant temperature boundary layer probe, TSI model 1218-T1.5. The constant wire temperature of 250°C is maintained using a two channel hot-wire anemometer, TSI model IFA-100. The hot wire signal is amplified and filtered by a signal conditioner, TSI model 157. In a typical run, a low pass filter is set at 5 kHz and high pass filter is set at 10 Hz. The offset and gain are set at 1 and 10, respectively.

The velocity and the turbulence intensity for each of the four turbulence generators are shown in Fig. 3. The velocity is quite uniform. The dimensionless power

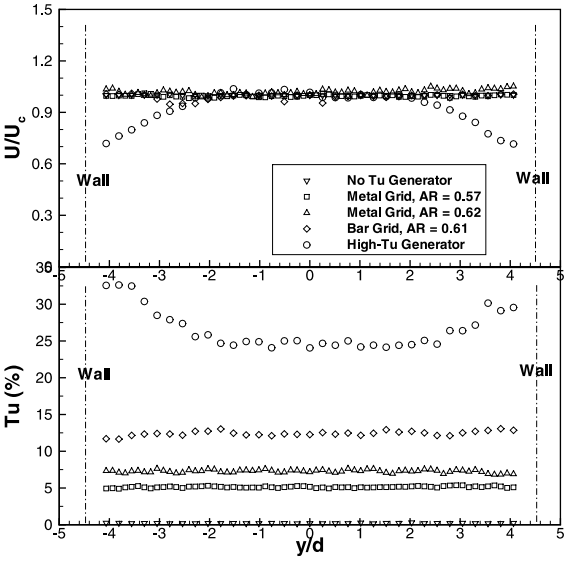

Fig. 3. Distribution of velocity and turbulence intensity at center of tunnel ($z/d = 0$) and location of cylinder center line ($x/d = 0$).

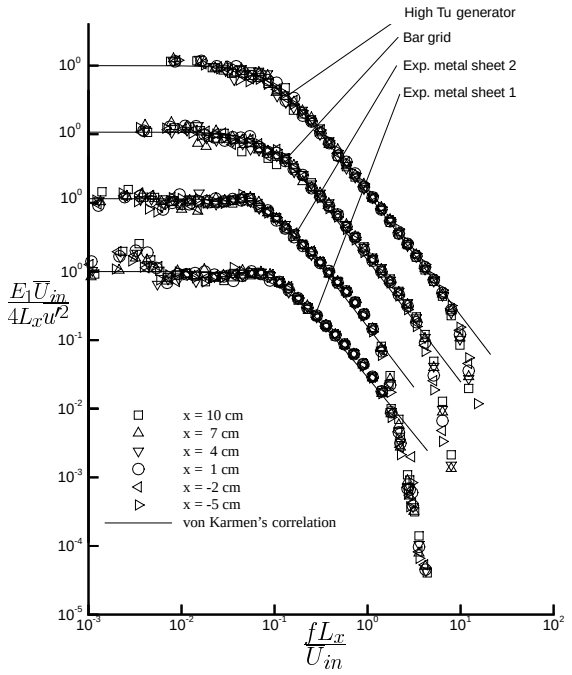

Fig. 4. Dimensionless power spectra of turbulence generators measured at $y/d = 0,\ z/d = 4.57$ for $Re = 60{,}000$.

spectra are shown in Fig. 4. If there are no continuous external sources of the energy for turbulent motion, turbulence decays by viscosity effects, which converts kinetic energy into internal energy. Viscosity also makes turbulence more homogeneous and less dependent on direction.

As shown in Fig. 5, the turbulence intensity decays somewhat in the streamwise direction but the longitudinal length scale increases. The turbulence intensity and longitudinal length scale (measured in the absence of the cylinder) at the position where the cylinder is placed ($x/d = 0,\ y/d = 0$, and $z/d = 4.57$) are summarized in Table 1.

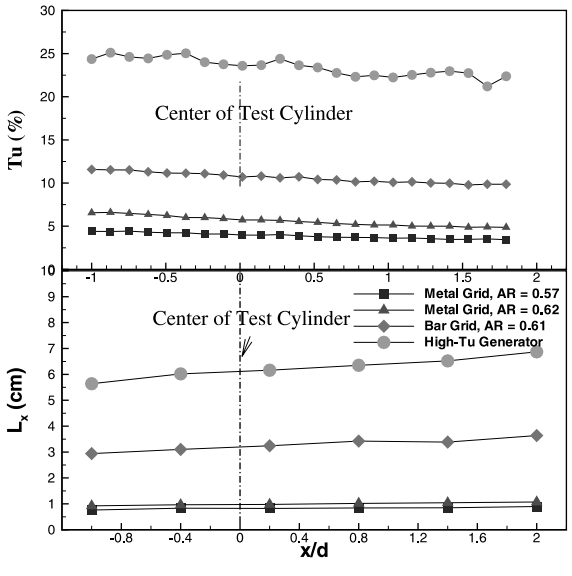

Fig. 5. Distribution of turbulence intensity and length scale in streamwise direction ($y/d = 0,\ z/d = 4.57$).

Table 1
Turbulence parameters at $x/d = 0,\ y/d = 0,\ z/d = 4.57$

Turbulence generator	AR (A_g/A_t)	Tu (%)	L_x (cm)
No turbulence generator	–	0.2	–
Expanded metal sheet 1	0.57	4.0	0.8
Expanded metal sheet 2	0.62	6.0	1.0
Bar grid	0.61	10.0	3.0
High turbulence generator	–	23.0	6.2

5. Results and discussion

5.1. Flow visualization

Flow visualization using an oil/lampblack mixture brushed on the cylinder surface indicates the flow field near the surface. In areas where the shear stress is strong, streaks are formed on the surface (gray region), while a streak-free black region is formed in areas where the shear stress is weak. Additionally, the flow pattern is observed using threads placed on the cylinder. All visualization tests are conducted at a Reynolds number of 6×10^4.

Flow visualization and Sherwood number distribution for $Re = 6 \times 10^4$ are presented in Fig. 6(a) for $Tu = 0.2\%$ and Fig. 6(b) for $Tu = 6\%$. A vertical black band at $\theta = 0°$ indicates the shear stress is small in this region.

At $Tu = 0.2\%$, the boundary layer separates at the end of the gray band ($\theta \approx 85°$). The Sherwood number gradually decreases from the front stagnation point until it reaches a minimum value near the laminar separation point. A black band from $\theta \approx 85°$ to $\theta \approx 150°$ corresponds to the hump in the mass transfer results. As reported by Scholten and Murray [11], a slight hump in the mass transfer coefficient distribution on the cylinder in the wake region indicates that there are secondary vortices in the reverse flow region. After the black band (from $\theta \approx 150°$), a second gray band appears due to the high shear stress caused by the irregular vortex shedding and the unsteady flow in the wake. A small gray band at $\theta \approx 90°$ may be caused by stationary vortices.

At $Tu = 6.0\%$, separation occurs at $\theta \approx 90°$ where the wall shear stress is very small and the black band starts.

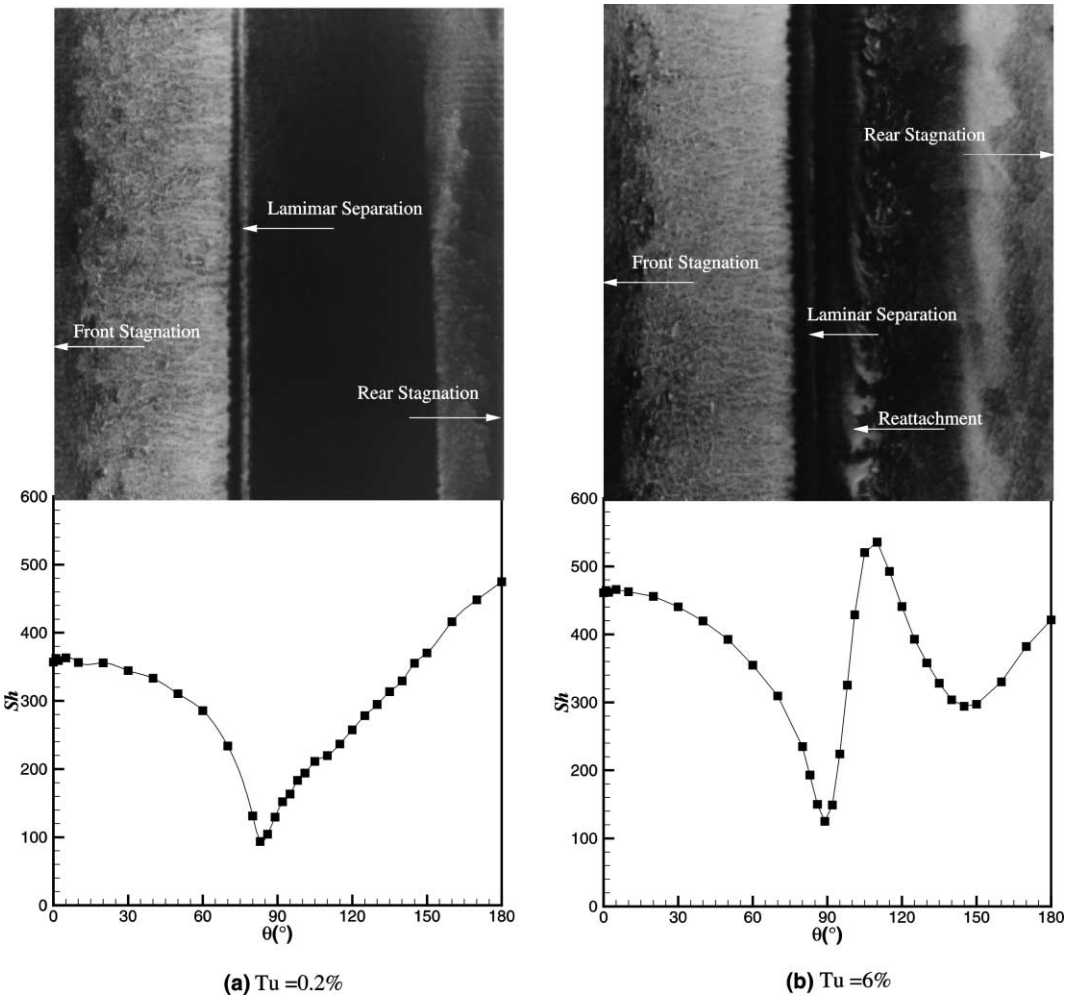

Fig. 6. Flow visualization at $Tu = 0.2\%$ and $Tu = 6\%$, $Re = 60{,}000$.

A minimum in Sherwood number occurs near this separation point. Downstream of the separation location a black band appears followed by a small gray band. This small gray band corresponds to the reattachment of the flow and high shear force. Mass transfer results show a peak at this location. The flow becomes unsteady and finally an apparently turbulent boundary layer separates at about 150° where the second gray band starts and the second minimum Sherwood number occurs. After the second separation point, the wall shear stress increases corresponding to the rear gray band.

5.2. Effect of Reynolds number at low free stream turbulence

Fig. 7 shows circumferential Sherwood number distributions for $Tu = 0.2\%$ at different Reynolds numbers. High values of Sherwood number occur at the front and rear stagnation points, $\theta = 0°$ and $\theta = 180°$, respectively. As θ increases from zero, the Sherwood number decreases gradually since the boundary layer thickens. Near the separation point, the local mass transfer drops sharply because of changes in the velocity profile in the boundary layer. The Sherwood number reaches a minimum value near where the laminar boundary layer separates. After separation, mass transfer increases monotonically to $\theta = 180°$. The increasing mass transfer in the rear part of the cylinder is due to the increased eddy effects in the wake region of the cylinder.

As expected, with an increase at the Reynolds number, the mass transfer increases. Over the range of Reynolds number studied the separation angle changes slightly, from 87° at $Re = 2.9 \times 10^4$ to 83° at $Re = 8.3 \times 10^4$ due to the increasing inertial effects. In the region from $\theta = 0°$ to $\theta = 70°$ near the minima, the curves

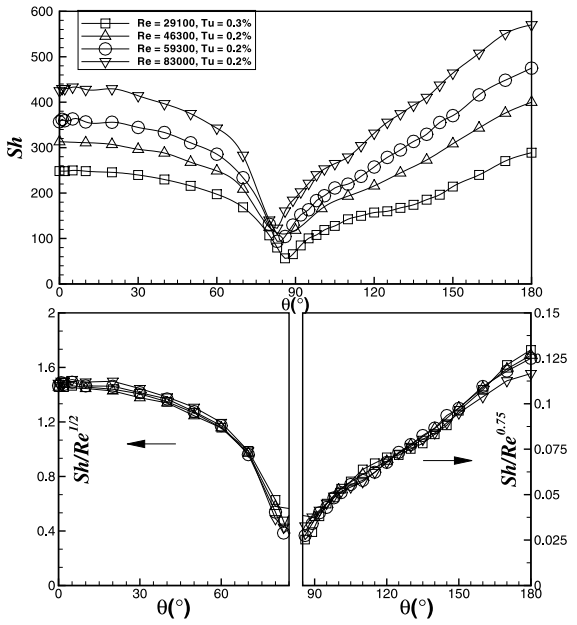

Fig. 7. Sherwood number and Sh/Re^n distributions for $Tu = 0.2\%$.

collapse on to one line when plotting $Sh/Re^{1/2}$, indicating a laminar boundary layer. Over most of the rear part of the cylinder, the Sherwood number appears to be proportional to $Re^{0.75}$.

5.3. Effect of free stream turbulence

In the range of Reynolds number investigated – all subcritical – the mass transfer changes significantly with free stream turbulence. Increases of Sherwood number at the front and rear stagnation point and average values are summarized in Table 2. As free stream turbulence increases, generally the mass transfer increases at the front stagnation point, but decreases at the rear stagnation point because of a weaker and smaller wake-width caused by the delay of separation. The pattern of the Sherwood number distribution changes considerably with free stream turbulence, a trend similar that found in the supercritical flow regime [21].

At $Re \approx 3 \times 10^4$, the mass transfer increases when the free stream turbulence increases as shown in Fig. 8. On the front part of the cylinder from 0° to 85° free stream turbulence clearly increases mass transfer in the "laminar" flow region. The boundary layer separates at about 85°. After separation, the free stream turbulence influence on the mass transfer depends on θ. The Sherwood numbers steeply increase after separation and reach a peak at 115° for $Tu = 11.7\%$. Turbulent mixing is the probable cause of this change. This peak, as indicated by the flow visualization shown in Fig. 6, is related to a reattachment of the flow. Fresh free stream fluid is drawn closer to the cylinder when flow reattaches causing high mass transfer. The boundary layer redevelops after the reattachment and becomes turbulent

Table 2
Change of Sherwood number at the front and rear stagnation point and average Sherwood number by the free stream turbulence effect

Re	Tu (%)	L_x (cm)	$Sh_{\theta=0}$	$Sh_{\theta=180}$	Sh_{avg}
31.2×10^3	0.3	–	265.1	299.1	205.2
46.7×10^3	0.2	–	323.2	402.7	265.6
59.3×10^3	0.2	–	362.2	496.1	308.1
82.2×10^3	0.2	–	425.0	570.2	369.8
Re	Tu (%)	L_x (cm)	$\triangle\left(Sh/\sqrt{Re}\right)$ (%) $\theta = 0$	$\triangle\left(Sh/\sqrt{Re}\right)$ (%) $\theta = 180$	$\triangle\left(Sh/\sqrt{Re}\right)$ (%) avg.
30.2×10^3	3.9	0.77	14	–1	5
47.7×10^3	3.8	0.77	23	–4	14
60.2×10^3	3.7	0.80	25	–8	18
79.3×10^3	3.6	0.80	47	6	43
30.2×10^3	5.7	0.96	12	10	11
47.4×10^3	5.6	0.96	26	–3	23
58.8×10^3	5.5	0.97	29	–12	25
80.7×10^3	5.3	1.00	47	–5	40
32.4×10^3	11.7	3.38	30	8	31
47.4×10^3	10.9	3.32	39	–2	36
62.7×10^3	10.5	3.40	44	–8	38
79.9×10^3	10.0	3.41	54	–9	40
31.1×10^3	23.7	6.32	39	0	41
45.6×10^3	23.4	6.21	43	–7	41
64.0×10^3	23.1	6.26	56	–10	47
71.2×10^3	22.4	6.32	61	–4	49

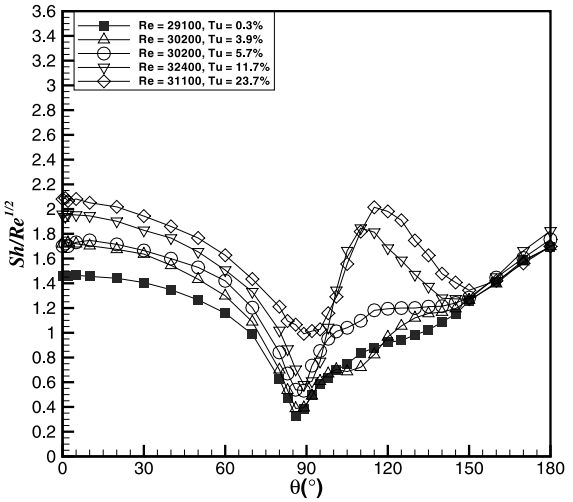

Fig. 8. $Sh/Re^{1/2}$ distribution at $Re \approx 30{,}000$.

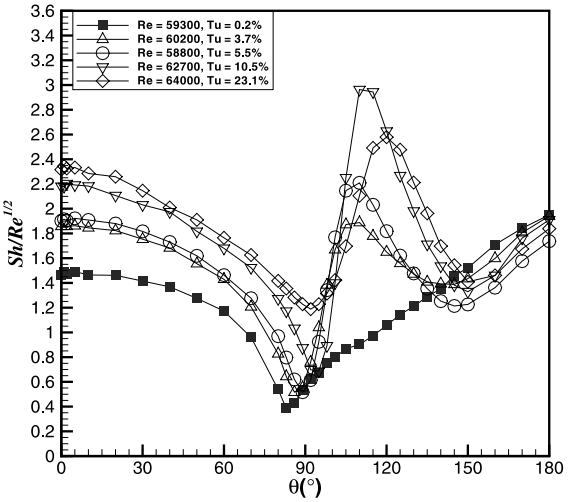

Fig. 9. $Sh/Re^{1/2}$ distribution at $Re \approx 60{,}000$.

as indicated by threads placed on the cylinder. The boundary layer keeps growing after reattachment and separates again at $\theta \approx 150°$ where the second minimum in Sherwood number and the second gray band from flow visualization (shown in Fig. 6) occur. The turbulent wake increases the Sherwood numbers, but this wake is weaker and has smaller width than that generated with low free stream turbulence due to the larger angle ($\theta \approx 150°$) at which this separation takes place. In the region after the first separation ($85° < \theta < 150°$), a small increase of the Sherwood number can be observed for $Tu \approx 4\%$. This indicates that, in this separated flow region, the change in flow characteristics depends on the level of free stream turbulence. There is no observable effect of free stream turbulence on mass transfer after 150° at this Re (Fig. 8). The turbulence generated by the eddies effect dominates the free stream turbulence.

On the front part of the cylinder, where the flow is laminar, free stream turbulence considerably influences the mass transfer rate, but in the region after the laminar separation ($\theta \approx 85°$), only high free stream turbulence ($Tu > 6\%$) has a significant effect on mass transfer (Fig. 8). Present results show agreement with the results from Lee et al. [10] who found that for turbulence intensity less than 5% at $Re = 4.9 \times 10^4$ the distribution of Sherwood number has a similar trend as with low turbulence intensity. For $Tu = 3.9\%$ the Sherwood number shows a hump after the laminar separation point. This hump, also found by Scholten and Murray [11], is apparently caused by a secondary vortex in the flow.

The Sherwood number distribution at $Re \approx 6 \times 10^4$ is shown in Fig. 9. At this higher Reynolds number, the presence of a peak after laminar separation occurs even at a moderate Tu of 4%. The laminar separation location moves downstream about 3°. A pronounced peak after the laminar separation is found. Reattachment occurs at $\theta \approx 110°$. The free stream turbulence effect is reversed after 145° where the highest mass transfer occurs for the base (lowest $Tu \approx 0.2\%$) flow.

We expect that flow patterns around a circular cylinder at Tu from $\approx 4\%$ to $\approx 23\%$ are similar at $Re = 6 \times 10^4$ because they have similar mass transfer distribution. On the front part of the cylinder mass transfer generally increases as turbulence intensity increases. Turbulence intensity still plays an important role in mass transfer in this region even when the length scale becomes large. It is noteworthy that the Sherwood number distributions on the rear part of the cylinder at $Tu \approx 23\%$ are lower than those at $Tu \approx 10\%$. It would be expected that the integral length scale may play a role in this result because the integral length scale ($L_x \approx 6.5$ cm for $Tu \approx 23\%$) is larger than the cylinder diameter ($L_x/d \approx 1.3$). At $Re \approx 6.0 \times 10^4$, $0.2\% < Tu < 23.7\%$ and 0.8 cm $< L_x <$ 6.3 cm the laminar separation location shifts downstream from $\theta \approx 85°$ to $\theta \approx 93°$. It is reasonable to expect a delay at the separation point since the momentum near the wall in a "turbulent-type" boundary layer is greater than in a laminar boundary layer.

5.4. Effect of Reynolds number at high free stream turbulence

Free stream turbulence has a stronger effect on mass transfer at higher Reynolds number due to the thinner boundary layer and a greater tendency for transition. As the turbulence intensity is increased from 0.2% to 4%, the mass transfer pattern (at $Re \approx 3.0 \times 10^4$) in the rear part of the cylinder does not change significantly (Fig. 10). No peak is present at $Tu \approx 4\%$ for this Re though

there are peaks in mass transfer in the rear part of the cylinder for larger Re. It is expected that mass transfer is strongly affected by the separation eddies around the cylinder at this Reynolds number. On the other hand, at low Reynolds number ($Re \approx 3 \times 10^4$) free stream turbulence strongly affects flow separation, if Tu is high enough. Such trends are apparent in Fig. 11 for $Tu \approx 11\%$.

Variation in mass transfer at the front stagnation point is shown in Fig. 12. The front stagnation point mass transfer is correlated with the parameter $TuRe(L_x/d)^{-0.5}$ which is similar to the parameter used in [15]. The correlation for the front stagnation point mass transfer can be written as

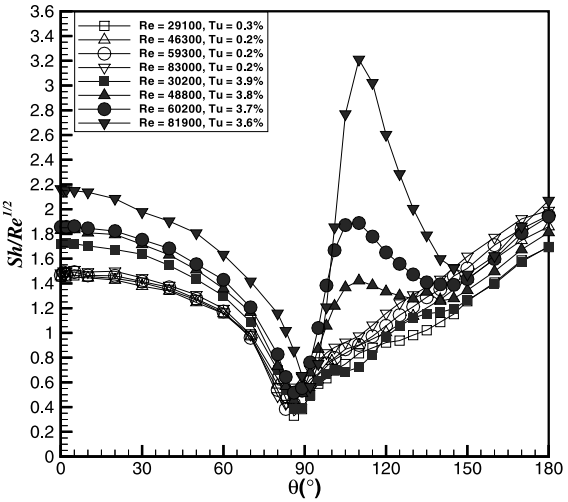

Fig. 10. Sherwood number distribution for $Tu \approx 0.2\%$ and 4%.

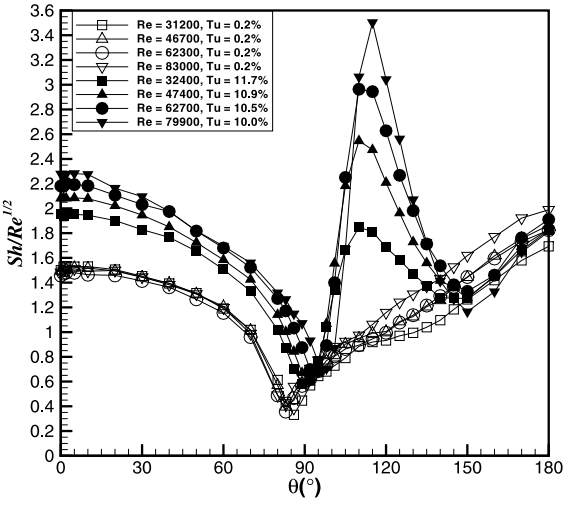

Fig. 11. Sherwood number distribution for $Tu \approx 0.2\%$ and 10%.

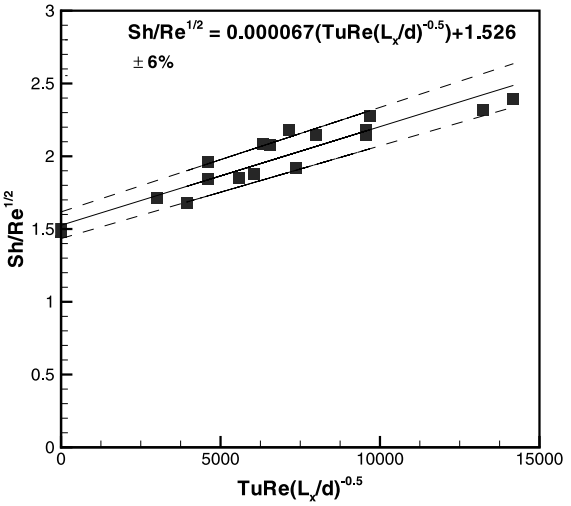

Fig. 12. $Sh/Re^{1/2}$ at front stagnation points at various free stream turbulence levels.

$$\frac{Sh_{\theta=0}}{Re^{1/2}} = 0.000067\left[TuRe\left(\frac{L_x}{d}\right)^{-0.5}\right] + 1.526. \tag{16}$$

5.5. Comparison with other heat and mass transfer results

The low free stream turbulence ($Tu = 0.2\%$) Sherwood number distributions in this study are compared with results from earlier studies in Fig. 13. Analytical solutions for laminar heat transfer are given by Eckert [22] and Frossling [23]. These solutions only apply to the front part of the cylinder, up to $\theta \approx 60°$. Some effects such as turbulence, even small level, and blockage make the present results somewhat higher than the theoretical predictions.

By the analogy between heat and mass transfer, $Sh = Nu$ if $Pr = Sc$. For $Pr \neq Sc$ we assume $Nu \propto Pr^n$, $Sh \propto Sc^n$ and

$$\frac{Sh}{Nu} = \left[\frac{Sc}{Pr}\right]^n, \tag{17}$$

where $n = 1/3$ for laminar flow. For naphthalene sublimation, $Sc \approx 2.28$ and for air $Pr \approx 0.71$ in the studies considered. The mass transfer results are converted to equivalent heat transfer results using Eq. (17).

On the front part of the cylinder the present results show good agreement with the heat transfer results from [24] and [21]. There are large discrepancies with the measurements of Zukauskas and Ziugzda [25].

The mass transfer results of [10,26–28] are also presented in Fig. 13. Good agreement is observed in the comparison of the mass transfer results on the front part of the cylinder before the separation point. On the rear part of the cylinder, both heat and mass transfer results

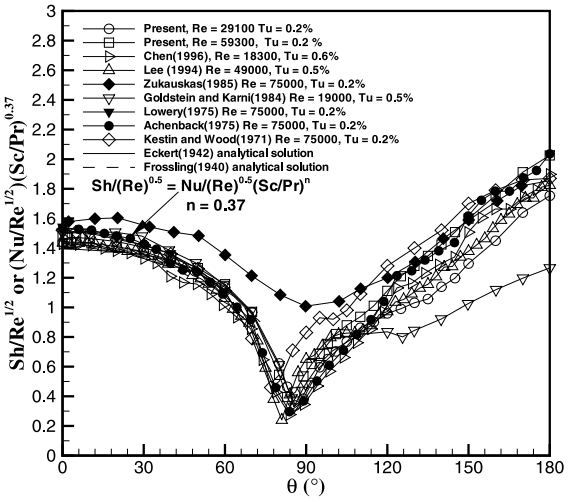

Fig. 13. Comparison with other results from heat and mass transfer measurements.

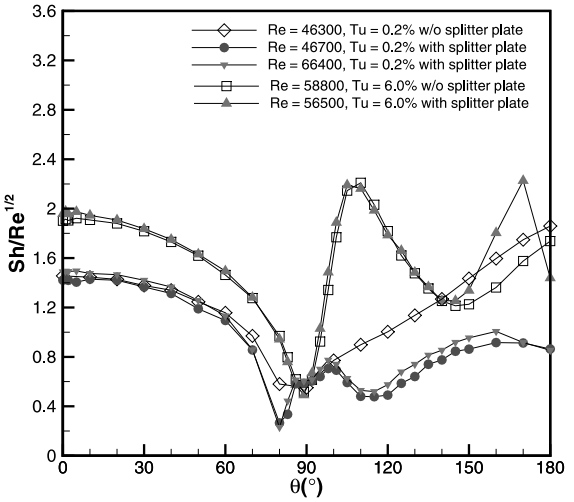

Fig. 14. Comparison between $Sh/Re^{1/2}$ distribution with and without a splitter plate.

show considerable differences. In the region after the separation point, from 85° to 120° the present results disagree with the heat transfer results from Achenbach [21]. The present results and the results from Chen [28], Lee et al. [10], Kestin and Wood [26] clearly show a small hump occurring in this region. This indicates that there may be secondary vortices in the reverse flow region.

5.6. Effect of a splitter plate on local mass transfer

The flow in the wake region after separation is unsteady. If the separation vortices are reduced, the mass transfer on the rear part of the cylinder should decrease. This can be accomplished by placing a splitter plate behind the test cylinder. Tests were performed with an 8 mm thick and 20 cm long splitter plate placed behind the rear stagnation line of the cylinder. The gap between the naphthalene surface of the cylinder and the splitter plate is 1 mm.

Results with and without a splitter plate are presented in Fig. 14. On the front part of the cylinder, the values of the Sherwood numbers are similar when $Tu = 0.2\%$; the splitter plate does not affect the mass transfer in the laminar flow region. From the separation point, $\theta \approx 85°$ to $\theta \approx 105°$, the mass transfer with the splitter plate increases. The mass transfer drops from $Sh/Re^{1/2} \approx 0.7$ to $Sh/Re^{1/2} \approx 0.4$ at $\theta \approx 115°$ and gradually increases toward the rear stagnation point. The smaller mass transfer is due to a reduction of the separation vortices. From $\theta \approx 170°$ to $\theta \approx 180°$, the mass transfer decreases again because of the weak flow caused by the splitter plate which covers that surface area. At higher free stream turbulence, $Tu \approx 6\%$, generally, the distributions of the Sherwood number with and without a splitter plate are similar. The splitter plate has a small effect on mass transfer only after the reattachment point ($\theta \approx 90°$). Mass transfer is primarily affected by the free stream turbulence. At $\theta > 150°$ the physical presence of the splitter plate results in a peak at $\theta \approx 170°$ due to a strong local vortex near the corner between the cylinder and the splitter plate.

6. Summary and conclusions

The present investigation provides information about the effects of high free stream turbulence on local mass transfer from a circular cylinder. Flow visualization using an oil/lampblack mixture gives information on the local wall shear stress. Local mass transfer is obtained using the naphthalene sublimation technique. The effect of a splitter plate on local mass transfer is also investigated. The following conclusions can be drawn.

1. The front stagnation line Sherwood number increases as free stream turbulence increases. In the experimental range studied, the stagnation point Sherwood number increases about 60% as free stream turbulence intensity increases at the highest Re studied from 0.2% to 23%. In contrast, the rear stagnation point mass transfer is only slightly affected by the free stream turbulence and is generally reduced by the free stream turbulence.
2. In the laminar boundary-layer region, increased free stream turbulence increases the mass transfer rate. The amount of the increase decreases as θ and the

boundary layer thickness increase. A small increase is found near the laminar separation point.

3. Free stream turbulence strongly affects the flow around a cylinder. The characteristics of subcritical flow with high free stream turbulence appear similar to those with supercritical flow. It is expected that the transition Reynolds number is essentially reduced to a lower value. However, at low Reynolds number, higher levels of free stream turbulence are needed to alter the flow characteristics.
4. After the laminar separation point, there is a peak in the distribution of Sherwood number when high free stream turbulence is present. Mass transfer increases because of the onset of a turbulent boundary layer and reaches a maximum value near the location where the flow reattaches to the cylinder. The laminar separation location moves downstream as the level of free stream turbulence increases. In the range of Reynolds number from 3.0×10^4 to 8.3×10^4 and Tu from 0.2% to 23.7% the laminar separation location shifts downstream from $\theta \approx 85°$ to $\theta \approx 93°$.
5. Mass transfer in the region downstream of the reattachment point for $Tu = 22\%$ is less than for $Tu = 10\%$. It is expected that, at a particular Reynolds number, the length scale may play an important role in the mass transfer in this regime. A lower mass transfer rate at high free stream turbulence than at low turbulence level can be observed downstream of the second minimum in Sherwood number. The vortex strength and wake width in that region decrease perhaps due to the turbulent separation at high free stream turbulence.
6. A splitter plate strongly affects the local mass transfer downstream of the separation point at low free stream turbulence. Mass transfer is reduced in that region due to the elimination of the alternating separation vortices. There is little or no effect of a splitter plate on mass transfer if the free stream turbulence is high; then the mass transfer distribution depends on the level of free stream turbulence.

Acknowledgements

Support from the Engineering Research Program of the Office of Basic Energy Science at the US Department of Energy and from the Thai Government in the form of a fellowship for S. Sanitjai is gratefully acknowledged.

References

[1] V.T. Morgan, The overall convective heat transfer from smooth circular cylinders, Adv. Heat Transfer 11 (1975) 199–264.
[2] W.H. Giedt, Effect of turbulence level of incident air stream on local heat transfer and skin friction on a cylinder, J. Aeronaut. Sci. 18 (1951) 725–730.
[3] W.M. Bollen, Effect of turbulence on the heat transfer coefficient distribution around a cylinder normal to air flow, Master's Thesis, Oregon State College, Corvallis, OR, 1949.
[4] G.M. Zapp, The effect of turbulence on local heat transfer coefficients around a cylinder normal to an air stream, Master's Thesis, Oregon State College, Corvallis, OR, 1950.
[5] M. Morkovin, Flow around circular cylinders – a kaleidoscope of challenging fluid phenomenon, ASME Symposium of Fully Separated Flows, 1964, pp. 102–108.
[6] R.A. Seban, The influence of free stream turbulence on the local heat transfer from cylinders, J. Heat Transfer 82 (1960) 101–107.
[7] J. Kestin, P. Maeder, Influence of turbulence on transfer of heat from cylinders, NACA TN 4018, 1956.
[8] J. Kestin, P. Maeder, H. Wang, On boundary layers associated with oscillating streams, Appl. Sci. Res. 10 (1960) 1–22.
[9] A.A. Zukauskas, I.I. Zyugzda, V.Y. Survila, Effect of turbulence on heat transfer from cylinders in crossflow at critical Reynolds numbers, Heat Transfer Sov. Res. 10 (5) (1978) 1–8.
[10] J.S. Lee, D.K. Sohn, T.H. Lee, Simultaneous effects of free-stream turbulence intensity and integral length scale on mass transfer about a cylinder, Exp. Thermal Fluid Sci. 9 (2) (1994) 225–232.
[11] J.W. Scholten, D.B. Murray, Unsteady heat transfer and velocity of a cylinder in cross flow – I. Low free stream turbulence, Int. J. Heat Mass Transfer 41 (10) (1998) 1139–1148.
[12] B.V. Zijnen, Heat transfer from horizontal cylinders to a turbulent air flow, Appl. Sci. Res. 7 (1957) 205–223.
[13] N.R. Yardi, S.P. Sukhatme, Effects of turbulence intensity and integral length scale of a turbulent free stream on forced convection heat transfer from a circular cylinder in cross flow, in: Proceedings of the Sixth International Heat Transfer Conference, Toronto, Canada, 1978, pp. 347–352.
[14] S. Torii, W.J. Yang, Effects of the length scale of free-stream turbulence and cylinder size on local heat transfer in laminar separated flows, Exp. Heat Transfer 6 (2) (1993) 175–187.
[15] G.J. Van Fossen, R.J. Simoneau, C.Y. Ching, Influence of turbulence parameters, Reynolds number, and body shape on stagnation-region heat transfer, J. Heat Transfer 117 (3) (1995) 597–603.
[16] M. Smith, A. Kuethe, Effects of turbulence on laminar skin friction and heat transfer, Phys. Fluids 9 (1966) 2337–2344.
[17] F.E. Ames, Heat transfer with high intensity, large scale turbulence: the flat plate turbulent boundary layer and the cylindrical stagnation point, Ph.D. Thesis, Stanford University, Stanford, CA, 1990.
[18] H.P. Wang, Local mass transfer from a turbine blade: influence of high turbulence with large length scale on heat/mass transfer, Ph.D. Thesis, University of Minnesota, Minneapolis, MN, 1997.
[19] R.J. Goldstein, H.H. Cho, A review of mass transfer measurements using naphthalene sublimation, Exp. Thermal Fluid Sci. 10 (1995) 416–434.

[20] H.W. Coleman, W.G. Steele, Experimentation and Uncertainty Analysis for Engineers, Wiley, New York, 1989.
[21] A. Achenbach, Total and local heat transfer from a smooth circular cylinder in cross-flow at high Reynolds number, Int. J. Heat Mass Transfer 18 (12) (1975) 1387–1396.
[22] E.R.G. Eckert, Die bereshnung des warmeuberganges in der laminaren grenzschicht umstromter korper, VDI-Froschungshefl 416 (1942) 1–26.
[23] N. Frossling, Evaporation, heat transfer, and velocity distribution in two dimensional and rotationally symmetrical laminar boundary-layer flow, Acta Univ. Lund: English Translation, NACA TM 1432, 1958.
[24] G.W. Lowery, R.I. Vachon, The effect of turbulence on heat transfer from heated cylinders, Int. J. Heat Mass Transfer 18 (11) (1975) 1229–1242.
[25] A. Zukauskas, J. Ziugzda, Heat Transfer of a Cylinder in Crossflow, Hemisphere, New York, 1985.
[26] J. Kestin, R.T. Wood, The influence of turbulence on mass transfer from cylinders, J. Heat Transfer 93 (4) (1971) 321–327.
[27] R.J. Goldstein, J. Karni, The effect of a wall boundary layer on local mass transfer from a cylinder in crossflow, J. Heat Transfer 106 (2) (1984) 260–267.
[28] S.B. Chen, Experimental study of flow and local measurement heat/mass transfer from single cylinders and array of short pin-fins in crossflow, Ph.D. Thesis, University of Minnesota, Minneapolis, MN, 1996.